Amorphous-Carbon-Supported Ultrasmall TiB₂ Nanoparticles With High Catalytic Activity for Reversible Hydrogen Storage in NaAlH₄

Xin Zhang[1], Xuelian Zhang[1], Zhuanghe Ren[1], Jianjiang Hu[2], Mingxia Gao[1], Hongge Pan[1] and Yongfeng Liu[1]*

[1] State Key Laboratory of Silicon Materials and School of Materials Science and Engineering, Zhejiang University, Hangzhou, China, [2] School of Chemistry and Chemical Engineering, Yantai University, Yantai, China

In this paper, we report amorphous-carbon-supported TiB₂ nanoparticles having sizes of 2–4 nm (nano-TiB₂@C) as highly active catalysts for hydrogen storage in NaAlH₄. Nano-TiB₂@C was synthesized by a simple calcination at 550°C with Cp₂TiCl₂ and MgB₂ (molar ratio of 1:1) as precursors. The addition of 7 wt% nano-TiB₂@C reduced the onset dehydrogenation temperature of NaAlH₄ by 100 to 75°C. A practically available hydrogen capacity of 5.04 wt% could be desorbed at 140°C within 60 min, and completely hydrogenated at 100°C within 25 min under a hydrogen pressure of 100 bar. Notably, the hydrogen capacity was almost unchanged after 20 cycles, which shows the stable cyclability, considerably higher than those of structures catalyzed by Ti halides or TiO₂. The stable catalytic function was closely related to the in-situ-formed Ti–Al alloy, which considerably facilitated the dissociation and recombination of H–H and Al–H bondings.

Keywords: hydrogen storage, complex hydrides, alanates, catalyst doping, cycling stability

INTRODUCTION

Considering its high energy density, abundance, small weight, and environmental friendliness, hydrogen could provide a considerably cleaner and more sustainable society in the future (Schlapbach and Züttel, 2001). However, various challenges should be overcome to achieve the storage of hydrogen in a safe, efficient, and economic manner (Eberle et al., 2009). Metal complex hydrides composed of metal cations and complex anions (i.e., alanates, borohydrides, and amides) can store considerably more hydrogen than traditional interstitial hydrides, and thus have attracted increasing interest in recent years (Orimo et al., 2007; Jain et al., 2010). In particular, sodium alanate (NaAlH₄) is considered a promising solid medium for hydrogen storage because of its suitable thermodynamics, relatively low desorption temperature, and good reversibility (Li et al., 2013a; Liu et al., 2018). Theoretically, NaAlH₄ contains 7.5 wt% H₂ which is obtained in a three-step process.
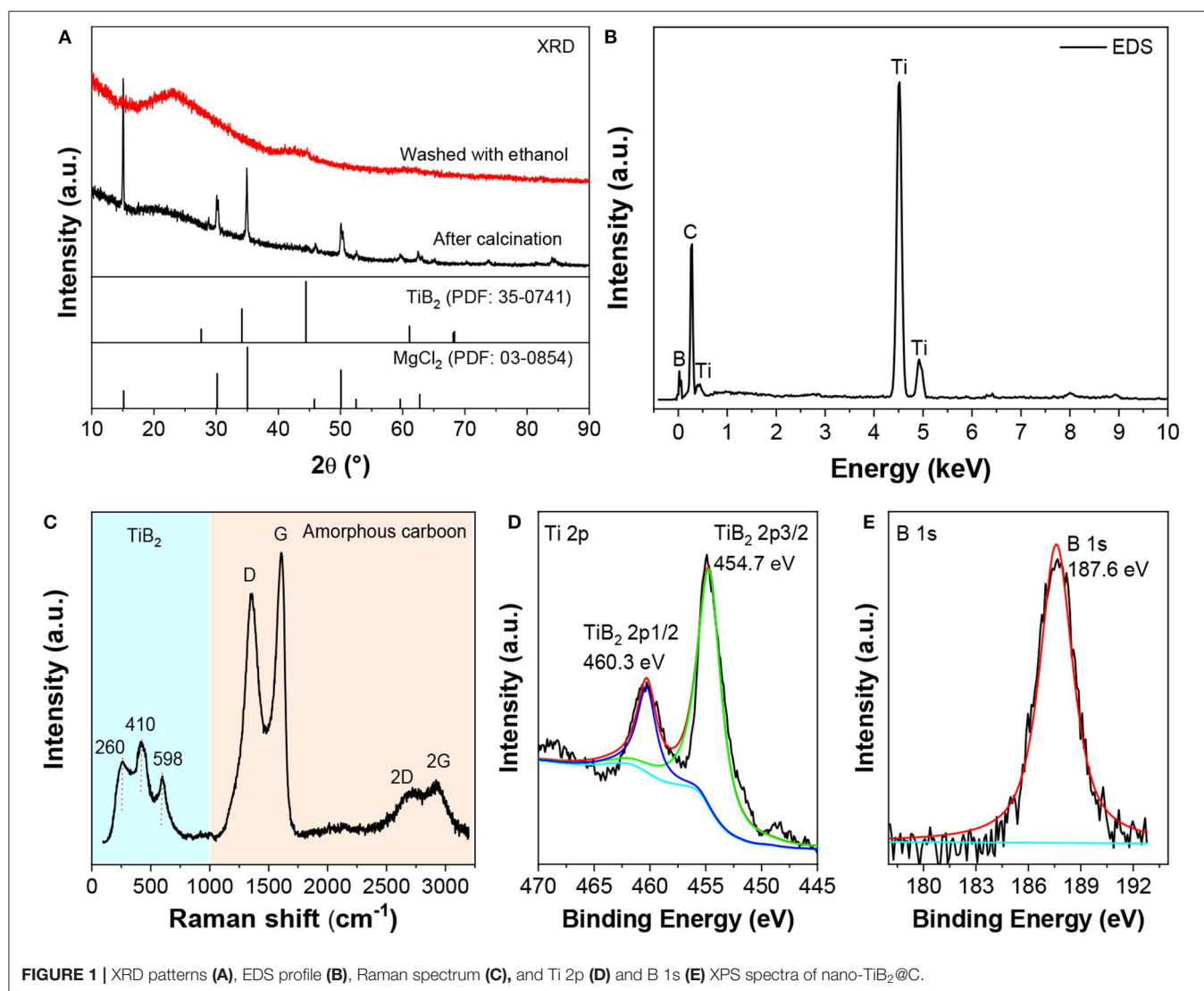
$$NaAlH_4 \leftrightarrow \frac{1}{3}Na_3AlH_6 + \frac{2}{3}Al + H_2 \leftrightarrow NaH + Al + \frac{3}{2}H_2 \leftrightarrow Na + Al + 2H_2 \tag{1}$$
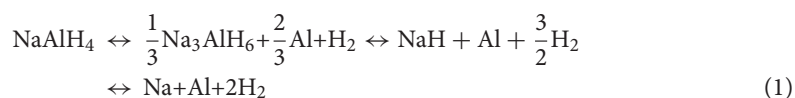
FIGURE 1 | XRD patterns **(A)**, EDS profile **(B)**, Raman spectrum **(C)**, and Ti 2p **(D)** and B 1s **(E)** XPS spectra of nano-TiB$_2$@C.

However, only 5.6 wt% H$_2$ from the first two steps in the above equation can be utilized for practical applications as the decomposition of NaH occurs at temperatures over 400°C (Li et al., 2013a), too high for hydrogen storage.

Several strategies have been developed to improve the hydrogen storage properties of complex hydrides, such as catalyst doping (Frankcombe, 2012; Liu et al., 2018), cations substituting (Jain et al., 2010; Fang et al., 2011; Mo and Jiang, 2018), fabrication of reactive composites (Vajo et al., 2005; Ding et al., 2015; Mustafa et al., 2018), and nanostructuring (Ding and Shaw, 2019; Ding et al., 2019a, 2020). Recently, Shaw's group have developed a ball milling process with aerosol spraying to fabricate a nanocomposite of LiBH$_4$ and MgH$_2$ and successfully achieved the dual-tuning effects of the thermodynamics and kinetics of LiBH$_4$ (Ding et al., 2019b). Regarding NaAlH$_4$, numerous studies have shown that the addition of appropriate catalysts is crucial for a reduction in its hydrogen storage operation temperatures (Liu et al., 2018). In 1997, for the first time,

Bogdanović and Schwickardi have reported a reduction (higher than 80°C) in desorption temperature of NaAlH$_4$ by doping 2 mol% β-TiCl$_3$ (Bogdanović and Schwickardi, 1997). Since then, various Ti-based additives have been introduced into NaAlH$_4$, particularly Ti halides and oxides, the most investigated catalysts (Frankcombe, 2012). Using TiF$_3$, Wang et al. have reported a release of H$_2$ above 2.5 wt% at 120°C (Wang et al., 2005; Kang et al., 2007). Lee et al. observed superior catalytic activity for nano-TiO$_2$ over TiCl$_3$ because a nano-TiO$_2$-containing NaAlH$_4$ has released ~3 wt% H$_2$ at 150°C within 10 min while only 2.5 wt% H$_2$ has been released from a TiCl$_3$-doped sample (Lee et al., 2008). Moreover, complete hydrogen release from NaAlH$_4$ was realized with a nano-TiO$_2$/C composite catalyst at 140°C within 30 min, with up to an H$_2$ capacity of 4.5 wt% (Liu et al., 2016).

However, the introduction of high-electronegativity anions, such as O, F, Cl, and Br, has reduced the effective hydrogen capacity because these anions tend to combine with Na and/or Al and consume the active components of hydrogen storage.

Thus, methods to simultaneously achieve low dehydrogenation temperatures and high practical hydrogen capacities are required. In this regard, Ti-based compounds composed of low-electronegativity anions, such as TiN, TiC, and TiB$_2$, have come in sight for their catalytic activities. A reversible storage capacity of 4.9 wt% H$_2$ has been demonstrated within 16 cycles by doping TiN into NaAlH$_4$ (Bogdanovic et al., 2003). A NaAlH$_4$-2%TiN mixture has exhibited a capacity above 5 wt% H$_2$ at 250°C (Li et al., 2013b). A rod-shaped nano-TiN@C-N composite has reduced the hydrogen desorption temperature to 140°C with an H$_2$ capacity of 4.9 wt% (Zhang et al., 2018). Relatively high hydrogen capacity was also obtained for TiB$_2$-doped NaAlH$_4$ (Li et al., 2012a,b; Liu et al., 2014). However, only a limited reduction in dehydrogenation temperature has been attained

so far. Further increase in the catalytic effectiveness of TiB$_2$ is still desired.

In this study, we synthesized an amorphous-carbon-supported nanoparticulate TiB$_2$ (nano-TiB$_2$@C) by calcining a mixture of Cp$_2$TiCl$_2$ and MgB$_2$. The fabricated nano-TiB$_2$ has a size of 2–4 nm and exhibited a remarkable catalytic activity for the hydrogen storage reaction of NaAlH$_4$. A reduction in onset dehydrogenation temperature higher than 100°C was achieved using a 7 wt% nano-TiB$_2$@C, which provided a practically available hydrogen capacity of 5.04 wt%. Furthermore, almost no capacity loss was observed within 20 cycles, which is superior to the performances of reported TiB$_2$-modified samples. The chemical states of nano-TiB$_2$@C and corresponding catalytic mechanisms were analyzed.
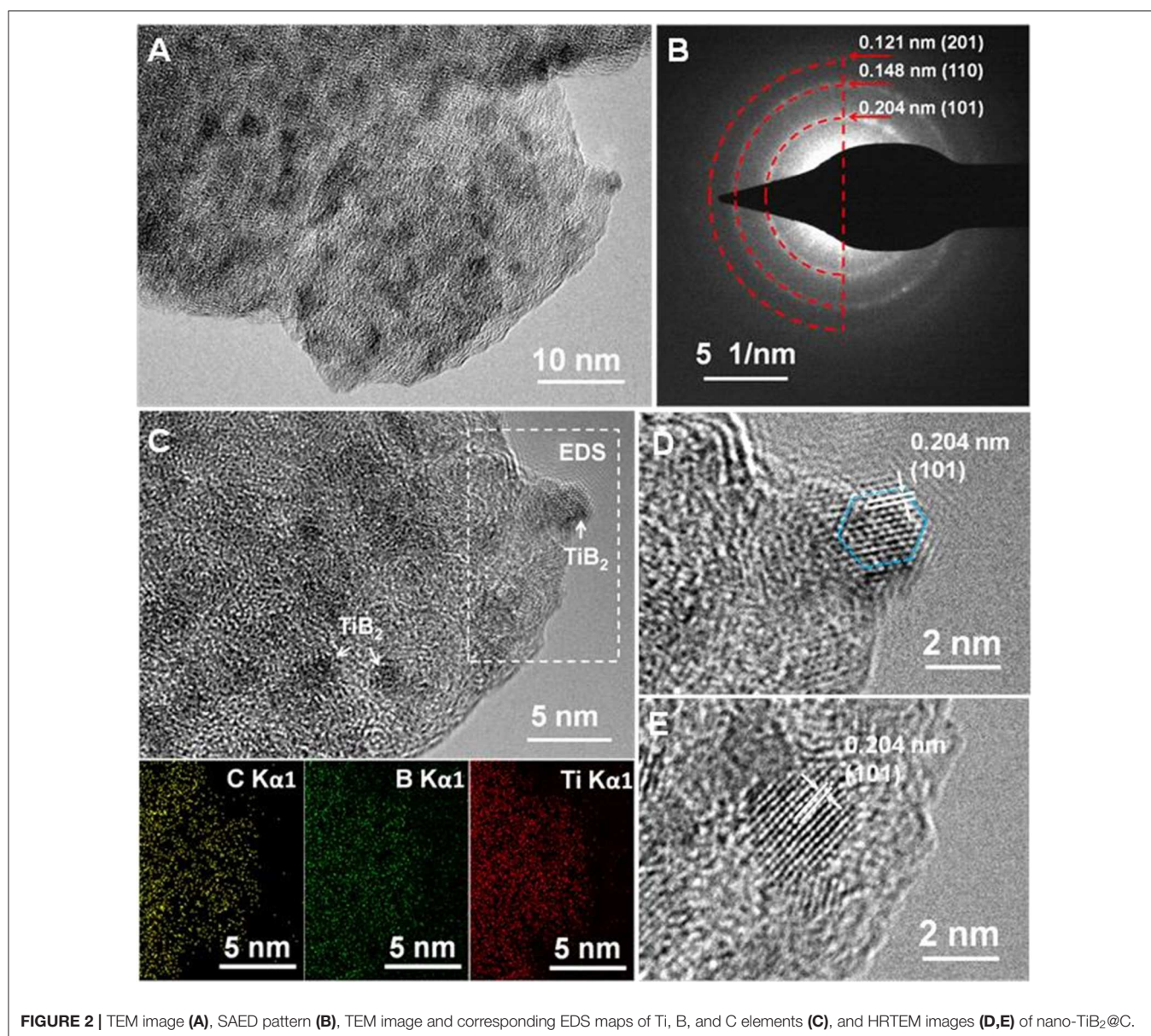

FIGURE 2 | TEM image (A), SAED pattern (B), TEM image and corresponding EDS maps of Ti, B, and C elements (C), and HRTEM images (D,E) of nano-TiB$_2$@C.
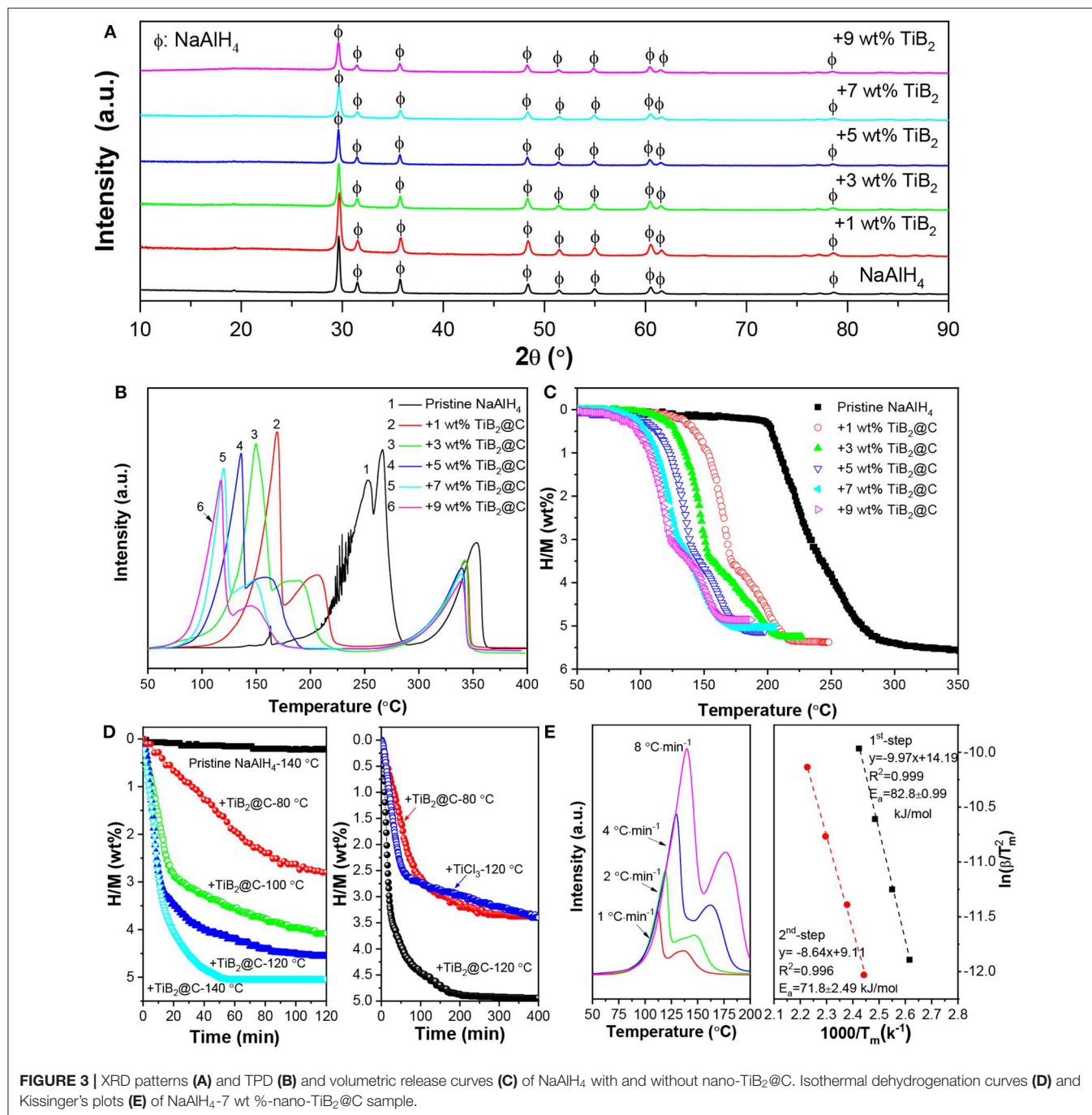
EXPERIMENTAL

Fabrication of Materials

All reagents and solvents were commercially available and used as received without further purification. Nano-TiB$_2$@C was synthesized by calcining a mixture of titanocene dichloride (Cp$_2$TiCl$_2$, 97%, Aladdin) and MgB$_2$ (97%, Alfa Aesar) with a molar ratio of 1:1 under an Ar atmosphere at 550°C for 2 h. The resultant powders were collected, washed twice with tetrahydrofuran (THF) to remove the byproduct MgCl$_2$, and

dried under vacuum at 150°C for 12 h to yield the nano-TiB$_2$@C composite.

Nano-TiB$_2$@C was mixed with NaAlH$_4$ (hydrogen storage grade, Sigma Aldrich) to evaluate its catalytic effectiveness. The weight percent of nano-TiB$_2$@C with respect to NaAlH$_4$ was designed to be 0, 1, 3, 5, 7, or 9 wt%. The sample mixing was carried out using a QM-3SP4 planetary ball mill under a hydrogen pressure of 50 bar. Approximately 1 g of the mixture was loaded into the milling jar inside an MBRAUN glovebox (Germany) filled with pure argon (H$_2$O
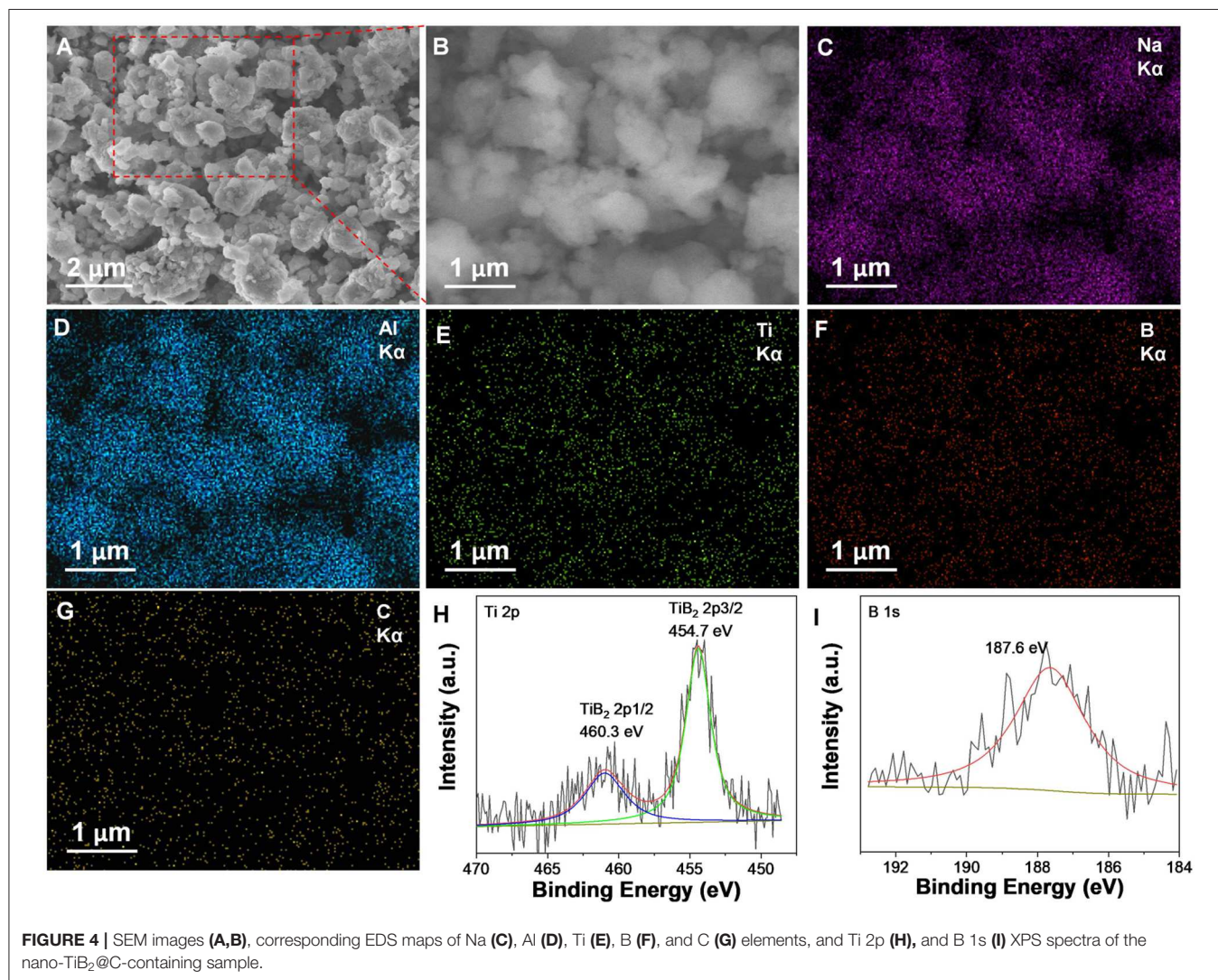

FIGURE 3 | XRD patterns (A) and TPD (B) and volumetric release curves (C) of NaAlH$_4$ with and without nano-TiB$_2$@C. Isothermal dehydrogenation curves (D) and Kissinger's plots (E) of NaAlH$_4$-7 wt %-nano-TiB$_2$@C sample.

FIGURE 4 | SEM images **(A,B)**, corresponding EDS maps of Na **(C)**, Al **(D)**, Ti **(E)**, B **(F)**, and C **(G)** elements, and Ti 2p **(H)**, and B 1s **(I)** XPS spectra of the nano-TiB$_2$@C-containing sample.

TABLE 1 | Comparison of desorption performances of catalyst-doped NaAlH$_4$ samples.

Catalyst	Non-isothermal desorption			Isothermal desorption			References
	On-set temperature (°C)	Terminal temperature (°C)	Capacity (wt%)	Temperature (°C)	Time (min)	H$_2$ release (wt%)	
TiB$_2$	150	300	5.3	150	900	3	Li et al., 2012a
TiB$_2$	75	250	4.9	120	400	3.2	Li et al., 2012b
TiCl$_3$	100	210	4.7	150	240	4.5	Lee et al., 2008
Nano-TiO$_2$	125	225	5	150	240	4.7	
TiF$_3$	–	–	–	120	240	3.75	Wang et al., 2005
TiN	120	220	5.37	190	600	5.37	Li et al., 2013b
TiC	–	–	–	165	480	4.5	Fan et al., 2009
VCl$_3$	160	250	4	–	–	–	Naik et al., 2009
ScCl$_3$	150	225	4.3	–	–	–	Naik et al., 2009
This work	75	175	5.04	140	50	5.04	

and $O_2 < 1$ part per million). The ball-to-sample weight ratio was ~120:1. The mill rotated for 0.3 h in one direction, paused for 0.1 h, and then rotated in the reverse direction for another 0.3 h.

Characterization

The dehydrogenation was qualitatively evaluated using a home-developed temperature-programmed desorption (TPD) system attached to an online gas chromatograph (GC). The sample (~40 mg) was heated from room temperature to 400°C at 2°C min^{-1} with pure Ar as a carrier gas at a flow rate of 20 ml min^{-1}. Quantitative dehydrogenation and hydrogenation properties were evaluated using a home-developed Sieverts-type apparatus. Isothermal and non-isothermal measurements were performed on samples having masses of ~60 mg. In the non-isothermal experiments, a heating rate of 2°C min^{-1} and primary vacuum (~10^{-3} Torr) were used for dehydrogenation, while a heating rate of 1°C min^{-1} and hydrogen pressure of 100 bar were used for hydrogenation. In the isothermal measurements, the samples were rapidly heated to a desired temperature and kept at that temperature during the entire test.

X-ray diffraction (XRD, X'Pert Pro, Rigaku, Japan) with Cu K_α radiation (40 kV, 40 mA) was carried out for identification of phases. XRD patterns were acquired in a 2θ range of 10–90° with step increments of 0.05°. The sample powders were sealed in a custom-designed container with a window covered by Scotch tape to prevent air and moisture contaminations. An elemental analysis was performed using a Vario MICRO cube element analyzer (Elementer, Germany) to quantify the contents of Ti, B, and C elements. Scanning electron microscopy (SEM, Hitachi, S-4800) and transmission electron microscopy (TEM, FEI, Tecnai G2 F20 S-TWIN) were used for morphology observations. The distributions of elemental Ti, B, and C were identified using an energy-dispersive X-ray spectrometer (EDS) attached to the Tecnai G2 F20 S-TWIN TEM facility. X-ray photoelectron spectroscopy (XPS) analyses were carried out using a Kratos AXIS Ultra DLD spectrometer with a monochromatic Al K_α X-ray source at a base pressure of 6.8×10^{-9} Torr. Fitting was carried out suing the XPSPEAK41 software.

RESULTS AND DISCUSSIONS

The structure and composition of the fabricated nano-TiB_2@C were analyzed by XRD, EDS and XPS. The results are shown in
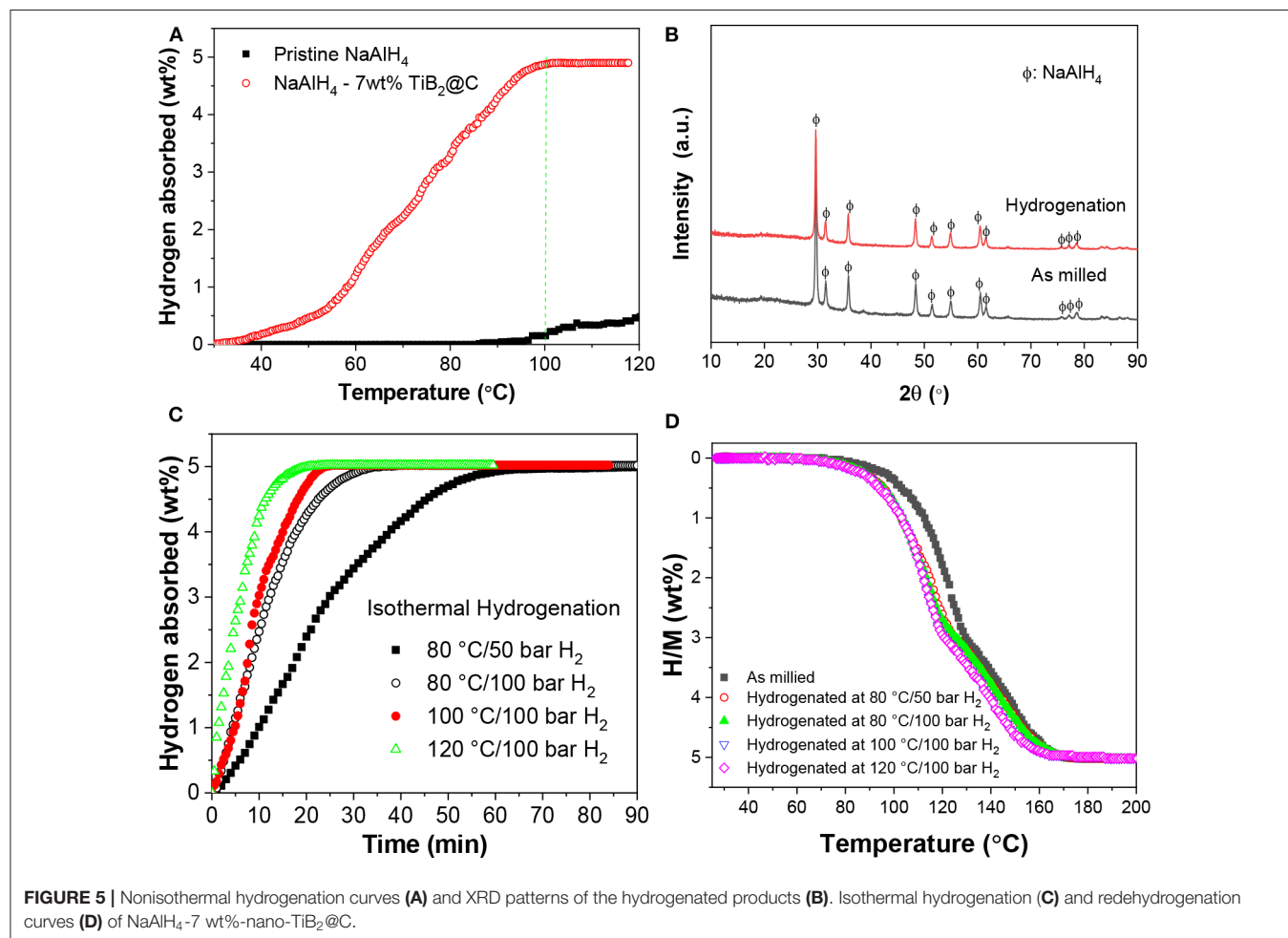
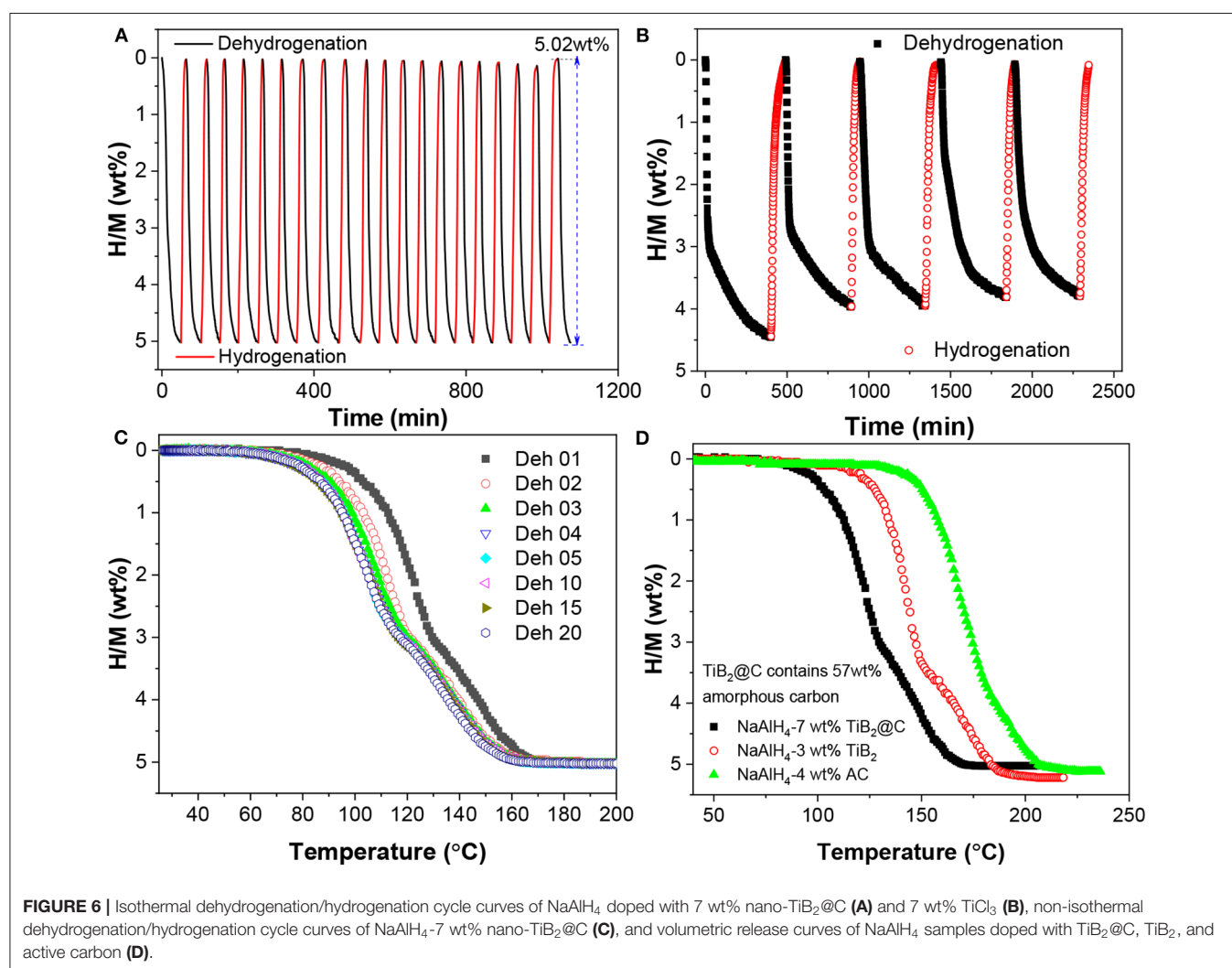

FIGURE 5 | Nonisothermal hydrogenation curves **(A)** and XRD patterns of the hydrogenated products **(B)**. Isothermal hydrogenation **(C)** and redehydrogenation curves **(D)** of $NaAlH_4$-7 wt%-nano-TiB_2@C.

Figure 1. The calcinated sample exhibited the diffraction peaks of MgCl$_2$ (**Figure 1A**). After the washing with THF, only a broad bump at 44.4° (2θ) was observed in the XRD profile. The low and broad peaks indicate low crystallization and/or small particle/grain sizes. Ti, B, and C were detected by EDS (**Figure 1B**). An element analysis shows that their weight ratio was ∼29:14:57, corresponding to a molar ratio of Ti and B of 1:2. A Raman spectrum analysis indicates that the elemental C was in its amorphous form (**Figure 1C**). Three characteristic peaks of TiB$_2$ were observed at 260, 410, and 598 cm^{-1} (Bača and Stelzer, 2008). The high-resolution XPS spectra (**Figures 1D,E**) show characteristic peaks of the Ti–B bonding at binding energies of 460.3/454.7 eV for Ti 2p and 187.6 eV for B 1s (Ding J. C. et al., 2019). Combining the XRD, EDS, and XPS results, we believe that TiB$_2$ and amorphous carbon were formed by calcining the mixture of Cp$_2$TiCl$_2$ and MgB$_2$.

TEM, HRTEM, EDS mapping, and selected-area electron diffraction (SAED) analyses were carried out. The TEM image (**Figure 2A**) shows a large number of black nanoparticles distributed in a gray matrix. The EDS mapping (**Figure 2B**) reveals that the small nanoparticles consisted of Ti and B, while the gray matrix was mainly C. The SAED pattern indicates (101), (110), and (201) planes assigned to TiB$_2$ (**Figure 2C**). The HRTEM images (**Figures 2D,E**) indicated an interplanar spacing of 0.204 nm, corresponding to the interplanar distance of the (101) planes of TiB$_2$. The particle sizes of the TiB$_2$ were ∼2–4 nm, part of which displayed clearly hexagon structures (**Figure 2D**). These results reveal nanoparticulate TiB$_2$ well-dispersed in the amorphous carbon matrix.

The resultant nano-TiB$_2$@C was mixed with NaAlH$_4$ by ball milling to test its catalytic effectiveness. After the ball milling, all samples exhibited very similar XRD patterns, as shown in **Figure 3A**. With the increase in amount of nano-TiB$_2$@C, the diffraction intensities of the NaAlH$_4$ phase slightly decreased. The SEM images reveal irregular solid particles with sizes of 200 nm−2 μm for 7 wt% nano-TiB$_2$@C-containing sample (**Figures 4A,B**). The EDS mapping results indicate relatively homogenous distribution of Ti, B, and C on NaAlH$_4$ particles (**Figures 4C–G**). Although no Ti-, B-, and C-containing phases were identified by XRD, possibly owing to their amorphous forms

FIGURE 6 | Isothermal dehydrogenation/hydrogenation cycle curves of NaAlH$_4$ doped with 7 wt% nano-TiB$_2$@C **(A)** and 7 wt% TiCl$_3$ **(B)**, non-isothermal dehydrogenation/hydrogenation cycle curves of NaAlH$_4$-7 wt% nano-TiB$_2$@C **(C)**, and volumetric release curves of NaAlH$_4$ samples doped with TiB$_2$@C, TiB$_2$, and active carbon **(D)**.
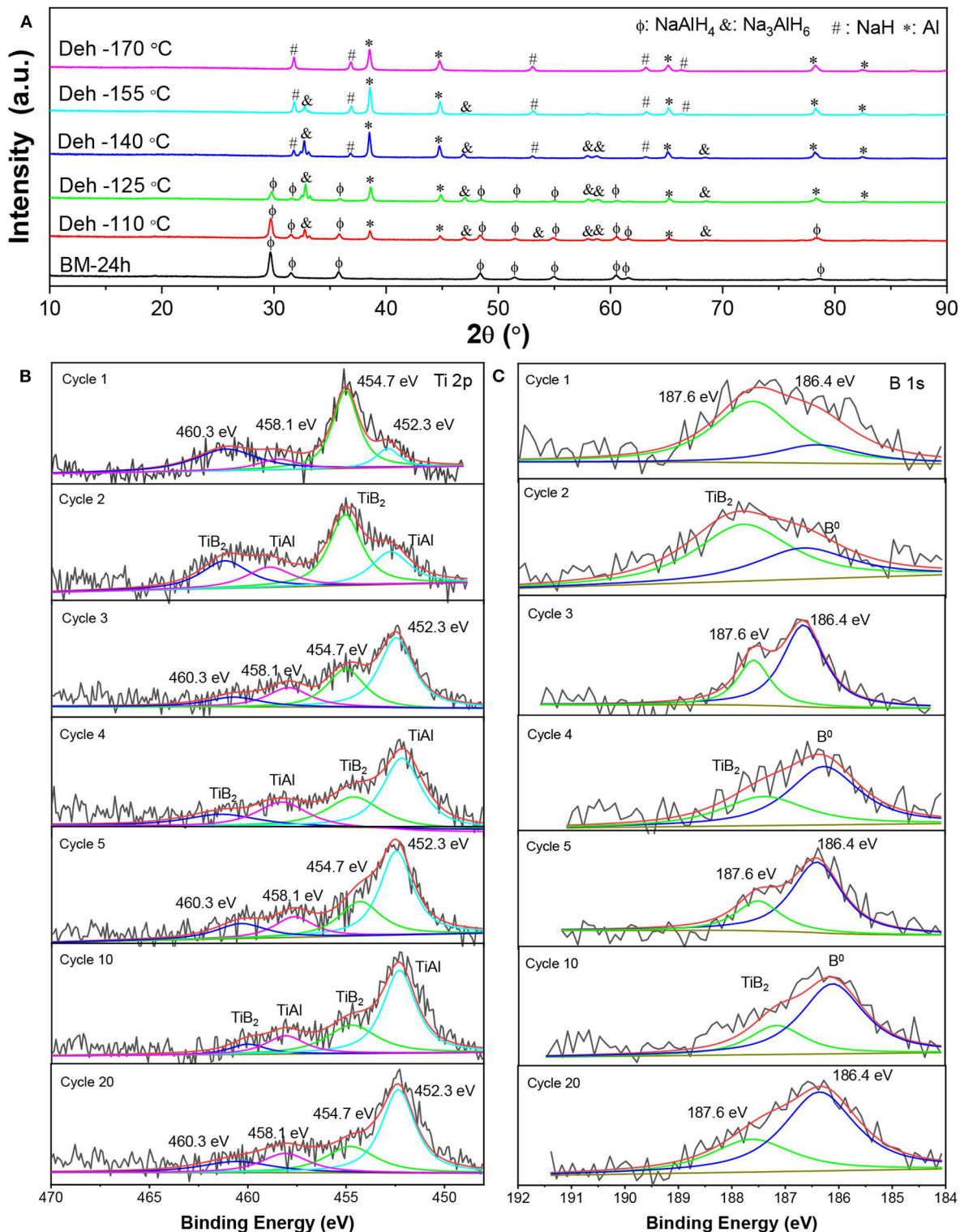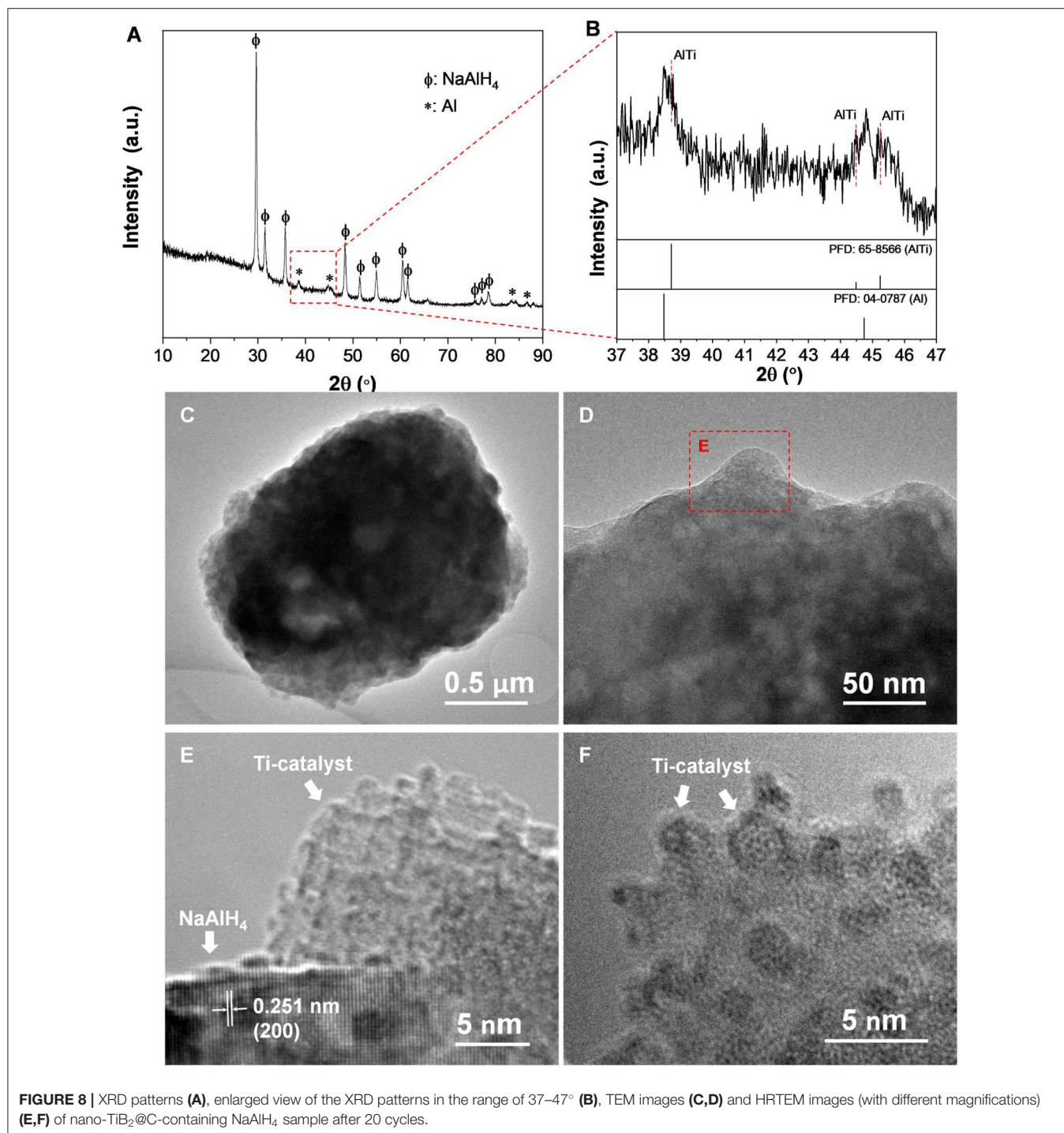
FIGURE 7 | XRD patterns as a function of the dehydrogenation temperature **(A)** and high resolution Ti 2p **(B)** and B 1s **(C)** XPS spectra of the nano-TiB$_2$@ C-containing sample after different numbers of dehydrogenation cycles.

(**Figure 3A**), the XPS results show Ti 2p and B 1s spectra assigned to TiB$_2$ with binding energies of 454.7/460.3 and 187.6 eV (**Figures 4H,I**), respectively, indicating the presence of TiB$_2$ upon the mixing with NaAlH$_4$. We therefore believe that nano-TiB$_2$@C was uniformly distributed into the NaAlH$_4$ matrix.

The nano-TiB$_2$@C-containing NaAlH$_4$ samples were subjected to TPD and volumetric measurements for qualitative

and quantitative characterization of their hydrogen storage performances. Three dehydrogenation peaks were observed in the TPD curves of all samples (**Figure 3B**), corresponding to the three-step decomposition process of NaAlH$_4$ with the increase in temperature (Equation 1). Furthermore, the nano-TiB$_2$@C-containing samples exhibited considerable low-temperature shifts. Upon the addition of 1 wt% nano-TiB$_2$@C,

FIGURE 8 | XRD patterns **(A)**, enlarged view of the XRD patterns in the range of 37–47° **(B)**, TEM images **(C,D)** and HRTEM images (with different magnifications) **(E,F)** of nano-TiB$_2$@C-containing NaAlH$_4$ sample after 20 cycles.

the dehydrogenation peak associated to the first dehydrogenation step (Equation 1) shifted from 255 to 169°C, a reduction of 86°C. The increase in nano-TiB$_2$@C content up to 7 wt% further reduced the start and end temperatures of the first-step decomposition to 75 and 118°C, 100 and 137°C lower than those of the pristine NaAlH$_4$, respectively. In addition to the slightly reduced peak intensities, the shape of TPD curve was almost unchanged with the further increase in content of nano-TiB$_2$@C. This result indicates that 7 wt% nano-TiB$_2$@C was optimal for the improvements in hydrogen storage performance of NaAlH$_4$.

Figure 3C shows volumetric release curves of the nano-TiB$_2$@C-modified samples. As expected, the 7 wt%-nano-TiB$_2$@C-containing sample exhibited the optimal dehydrogenation properties in terms of dehydrogenation temperature and hydrogen capacity in this study. Approximately 5.04 wt% of hydrogen was released in the temperature range of 75–175°C, which is remarkably superior to the performance of previously reported TiB$_2$-doped NaAlH$_4$ and other transition-metal-catalyzed NaAlH$_4$ structures (Table 1) (Wang et al., 2005; Lee et al., 2008; Fan et al., 2009; Naik et al., 2009; Li et al., 2012a,b, 2013b; Liu et al., 2014). In the isothermal test, the same amount of hydrogen (5.04 wt%) was released within 50 min at 140°C (Figure 3D). In contrast, <1 wt% of hydrogen was released from the pristine NaAlH$_4$ under the same conditions. At 120°C, the 7 wt%-nano-TiB$_2$@C-containing sample could desorb 4 wt% H$_2$ within 30 min, showing a much faster dehydrogenation kinetics than those of well-studied TiCl$_3$-modified NaAlH$_4$ (Figure 3D) (Bogdanović and Schwickardi, 1997; Naik et al., 2009). Even at 80°C, ~3.5 wt% H$_2$ could be desorbed, though a period of 400 min was required. These dehydrogenation kinetics outperform those of other TiB$_2$-doped NaAlH$_4$, which released only 2.79 wt% under the same conditions (Li et al., 2012b). Using the Kissinger's method (Kissinger, 1957), the apparent activation energies (E_a) were determined to be ~82.8 and 71.8 kJ/mol for the first and second dehydrogenation of the 7 wt%-nano-TiB$_2$@C-containing sample, respectively (Figure 3E), which are ~ 40% lower than those of pristine NaAlH$_4$ (Zhang et al., 2016) and is responsible for the remarkably reduced dehydrogenation temperatures.

The dehydrogenated samples were re-hydrogenated under an H$_2$ pressure of 100 bar. As shown in Figure 5A, the sample containing 7 wt%-nano-TiB$_2$@C started to absorb hydrogen at a temperature of 30°C, 70°C lower than that of the sample without doping. The hydrogenation was completed at 100°C in the non-isothermal test. The XRD analysis indicates that NaAlH$_4$ was formed after the full hydrogenation (Figure 5B). Isothermal hydrogenation under an H$_2$ pressure of 100 bar reveals that ~5.02 wt% of hydrogen recharged into the dehydrogenated 7 wt%-nano-TiB$_2$@C-containing sample within 35 min at 80°C, which provided full hydrogenation (Figure 5C). At 120°C, only 20 min were required to complete full hydrogenation, which shows the considerably faster kinetics. The follow-up dehydrogenation repeatedly resulted an H$_2$ capacity of 5.02 wt% (Figure 5D), which shows the good reversibility.

Figure 6A shows the cyclic stability of NaAlH$_4$-7 wt%-nano-TiB$_2$@C. Here, the dehydrogenation was conducted at 140°C in vacuum, while the hydrogenation took place at 100°C under an H$_2$ pressure of 100 bar. After 20 cycles, the available hydrogen capacity still remained at 5.02 wt%, which shows the stable recyclability. This cycling stability is superior to that of the well-studied TiCl$_3$-catalyzed NaAlH$_4$ (Figure 6B). In addition, a small but continuous reduction in onset dehydrogenation temperature was observed in the first four cycles (Figure 6C), which reflected the activation. This might correlate to some changes in catalytic active species during the initial de-/hydrogenation cycles. Further comparison reveals that hydrogen release from the nano-TiB$_2$@C-containing NaAlH$_4$ occurred at lower temperatures than those of samples with either TiB$_2$ or active carbon (AC) (Figure 6D), which shows the synergistic effect of TiB$_2$ and C, similarly to the previous observation for NaAlH$_4$ co-catalyzed by NbF$_5$ and single-walled carbon nanotubes (Mao et al., 2011, 2012).

Figure 7A shows XRD patterns of the dehydrogenated samples containing 7 wt% nano-TiB$_2$@C as a function of the temperature. The results indicate that with the increase in temperature, NaAlH$_4$ initially decomposed to Na$_3$AlH$_6$ and Al (110–140°C), which then led to the formation of NaH and Al (155–175°C) with the hydrogen release. We therefore believe that the presence of nano-TiB$_2$@C did not alter the dehydrogenation course of NaAlH$_4$. Notably, no Ti-containing species was identified by the XRD profiles. Subsequently, high-resolution Ti 2p and B 1s XPS spectra were acquired to understand the chemical states of TiB$_2$ (Figures 7B,C). Upon cycling, a 2p$_{3/2}$-2p$_{1/2}$ spin–orbit doublet at 452.3/458.1 eV emerged, and then became dominant in the Ti 2p XPS spectra (Figure 7B), which can be assigned to Ti–Al bonding (Mencer et al., 1991). Further XRD analysis confirms the presence of an AlTi alloy (Figures 8A,B). The AlTi alloy surface is favorable for the dissociation and recombination of H–H and Al–H bondings (Frankcombe, 2012; Liu et al., 2018). In contrast, the XPS peaks of Ti at 454.7/460.3 eV were largely reduced. On the other hand, the characteristic XPS peak of B^0 at 186.4 eV was also detected, which gradually increased in the initial four cycles. Thus, upon the de-/hydrogenation cycling, TiB$_2$ was gradually converted to Ti–Al and B, possibly reacting with NaAlH$_4$. This is crucial for the continuous reduction in dehydrogenation temperature of the nano-TiB$_2$@C-modified sample in the initial four cycles. The newly formed Ti–Al and B remained stable in the following cycles, which led to a good cycling stability, as shown in Figure 6A.

The nano-TiB$_2$@C-containing sample subjected to 20 cycles was used for a TEM observation. As shown in Figures 8C–F, a large number of Ti catalyst nanoparticles (sizes < 5 nm) were dispersed on the surface of the NaAlH$_4$ particle. Therefore, we believe that ultrasmall particles of TiB$_2$ as precursors facilitated the formation of ultrafine dispersive Ti–Al active species. The dispersive distribution of Ti catalysts provided the high catalytic activity for hydrogen storage in NaAlH$_4$, particularly for long-term cycling (Figure 4D).

CONCLUSIONS

In this work, nano-TiB$_2$@C below 5 nm was synthesized. Remarkable reduction in dehydrogenation and hydrognaiton temperatures was observed when adding 7 wt% nano-TiB$_2$@C to NaAlH$_4$. The hydorgen desorption started at a temperature of 75°C, which is lowered by 100°C compared to the pristine NaAlH$_4$. A practical hydrogen capacity of 5.04 wt% was determined, which was released within 50 min at 140°C. The rehydrogenation occurred at 30°C under a hydrogen pressure of 100 ba, and was completed at 100°C. Notably, no capacity loss was observed in the 20 cycles. During the initial de-/hydrogenation cycling, TiB$_2$ presumably reacted with NaAlH$_4$ and was converted to AlTi alloy and zero-valence B, which were well-dispersed on the surface of the NaAlH$_4$ particles, and consequently contributed to the high stable catalytic activity. These findings could facilitate the practical use of NaAlH$_4$ as a high-capacity reversible hydrogen storage medium.

DATA AVAILABILITY STATEMENT

All datasets generated for this study are included in the article/supplementary material.

AUTHOR CONTRIBUTIONS

XiZ and YL conceived the study and designed the experiments. XiZ, XuZ, and ZR carried out the material syntheses, characterization, and measurements. XiZ, YL, JH, MG, and HP analyzed the data. XiZ, JH, and YL wrote the manuscript.

FUNDING

REFERENCES

Bača, L., and Stelzer, N. (2008). Adapting of sol–gel process for preparation of TiB$_2$ powder from low-cost precursors. *J. Eur. Ceram. Soc.* 28, 907–911. doi: 10.1016/j.jeurceramsoc.2007.09.028

Bogdanovic, B., Felderhoff, M., Kaskel, S., Pommerin, A., Schlichte, K., and Schüth, F. (2003). Improved hydrogen storage properties of Ti–doped sodium alanate using titanium nanoparticles as doping agents. *Adv. Mater.* 15, 1012–1015. doi: 10.1002/adma.200304711

Bogdanović, B., and Schwickardi, M. (1997). Ti-doped alkali metal aluminium hydrides as potential novel reversible hydrogen storage materials. *J. Alloys Compd.* 253:112. doi: 10.1016/S0925-8388(96)03049-6

Ding, J. C., Lee, D., Mei, H. J., Zhang, T. F., Kang, M. C., Wang, Q. M., et al. (2019). Influence of Si addition on structure and properties of TiB$_2$-Si nanocomposite coatings deposited by high-power impulse magnetron sputtering. *Ceram. Int.* 45, 6363–6372. doi: 10.1016/j.ceramint.2018.12.122

Ding, Z., Li, H., and Shaw, L. (2019b). Solid-state hydrogen desorption of 2MgH$_2$ + LiBH$_4$ nano-mixture: a kinetics mechanism study. *J. Alloys Compd.* 806, 350–360. doi: 10.1016/j.jallcom.2019.07.218

Ding, Z., Li, H., and Shaw, L. (2020). New insights into the solid-state hydrogen storage of nanostructured LiBH4-MgH2 system. *Chem. Eng. J.* 385:123856. doi: 10.1016/j.cej.2019.123856

Ding, Z., Lu, Y., Li, L., and Shaw, L. (2019a). High reversible capacity hydrogen storage through Nano-LiBH$_4$ + Nano-MgH$_2$ system. *Energy Storage Mater.* 20, 24–35. doi: 10.1016/j.ensm.2019.04.025

Ding, Z., and Shaw, L. (2019). Enhancement of hydrogen desorption from nanocomposite prepared by ball milling MgH$_2$ with *in situ* aerosol spraying LiBH$_4$. *ACS Sustainable Chem. Eng.* 7, 15064–15072. doi: 10.1021/acssuschemeng.9b03724

Ding, Z., Zhao, X. Z., and Shaw, L. (2015). Reaction between LiBH$_4$ and MgH$_2$ induced by high-energy ball milling. *J. Power Sources* 293, 236–245. doi: 10.1016/j.jpowsour.2015.05.079

Eberle, U., Felderhoff, M., and Schüth, F. (2009). Chemical and physical solutions for hydrogen storage. *Angew. Chem. Int. Ed.* 48, 6608–6630. doi: 10.1002/anie.200806293

Fan, X. L., Xiao, X. Z., Hou, J. C., Zhang, Z., Liu, Y. B., Wu, Z., et al. (2009). Reversible hydrogen storage behaviors and microstructure of TiC-doped sodium aluminum hydride. *J. Mater. Sci.* 44, 4700–4704. doi: 10.1007/s10853-009-3726-y

Fang, Z. Z., Kang, X. D., Yang, Z. X., Walker, G. S., and Wang, P. (2011). Combined effects of functional cation and anion on the reversible dehydrogenation of LiBH$_4$. *J. Phys. Chem. C* 115, 11839–11845. doi: 10.1021/jp200137n

Frankcombe, T. J. (2012). Proposed mechanisms for the catalytic activity of Ti in NaAlH$_4$. *Chem. Rev.* 112, 2164–2178. doi: 10.1021/cr2001838

Jain, I. P., Jain, P., and Jain, A. (2010). Novel hydrogen storage materials: a review of lightweight complex hydrides. *J. Alloys Compd.* 503, 303–339. doi: 10.1016/j.jallcom.2010.04.250

Kang, X. D., Wang, P., and Cheng, H. M. (2007). Advantage of TiF$_3$ over TiCl$_3$ as a dopant precursor to improve the thermodynamic property of Na$_3$AlH$_6$. *Scripta Mater.* 56, 361–364. doi: 10.1016/j.scriptamat.2006.11.004

Kissinger, H. E. (1957). Reaction kinetics in differential thermal analysis. *Anal. Chem.* 29, 1702–1706. doi: 10.1021/ac60131a045

Lee, G. J., Shim, J. H., Cho, Y. W., and Lee, K. S. (2008). Improvement in desorption kinetics of NaAlH$_4$ catalyzed with TiO$_2$ nanopowder. *Int. J. Hydrogen Energy* 33, 3748–3753. doi: 10.1016/j.ijhydene.2008.04.035

Li, L., Qiu, F. Y., Wang, Y. J., Liu, G., Yan, C., An, C. H., et al. (2012a). Improved dehydrogenation performances of TiB$_2$-doped sodium alanate. *Mater. Chem. Phys.* 134, 1197–1202. doi: 10.1016/j.matchemphys.2012.04.022

Li, L., Qiu, F. Y., Wang, Y. J., Liu, G., Yan, C., An, C. H., et al. (2012b). Crystalline TiB$_2$: an efficient catalyst for synthesis and hydrogen desorption/absorption performances of NaAlH$_4$ system. *J. Mater. Chem. A* 22, 3127–3132. doi: 10.1039/c1jm14936a

Li, L., Wang, Y., Qiu, F. Y., Wang, Y. J., Xu, Y. N., An, C. H., et al. (2013b). Reversible hydrogen storage properties of NaAlH$_4$ enhanced with TiN catalyst. *J. Alloys Compd.* 566, 137–141. doi: 10.1016/j.jallcom.2013.03.088

Li, L., Xu, C. C., Chen, C. C., Wang, Y. J., Jiao, L. F., and Yuan, H. T. (2013a). Sodium alanate system for efficient hydrogen storage. *Int. J. Hydrogen Energy* 38, 8798–8812. doi: 10.1016/j.ijhydene.2013.04.109

Liu, C., Jiang, J. L., Huang, S. P., Wang, P., and Tian, H. P. (2014). Electronic and dehydrogenation properties of TiB$_2$ cluster-doped NaAlH$_4$ (101) surface: a first-principle approach. *Int. J. Hydrogen Energy* 39, 14178–14183. doi: 10.1016/j.ijhydene.2014.02.162

Liu, Y. F., Ren, Z. H., Zhang, X., Jian, N., Yang, Y. X., Gao, M. X., et al. (2018). Development of catalyst–enhanced sodium alanate as an advanced hydrogen–storage material for mobile applications. *Energy Technol.* 6, 487–500. doi: 10.1007/978-981-10-7677-0

Liu, Y. F., Zhang, X., Wang, K., Yang, Y. X., Gao, M. X., and Pan, H. G. (2016). Achieving ambient temperature hydrogen storage in ultrafine nanocrystalline TiO$_2$@C-doped NaAlH$_4$. *J. Mater. Chem. A* 4, 1087–1095. doi: 10.1039/C5TA09400C

Mao, J. F., Guo, Z. P., and Liu, H. K. (2011). Improved hydrogen sorption performance of NbF$_5$-catalysed NaAlH$_4$. *Int. J. Hydrogen Energy* 36, 14503–14511. doi: 10.1016/j.ijhydene.2011.08.055

Mao, J. F., Guo, Z. P., and Liu, H. K. (2012). Enhanced hydrogen storage properties of NaAlH$_4$ co-catalysed with niobium fluoride and single-walled carbon nanotubes. *RSC Adv.* 2, 1569–1576. doi: 10.1039/C1RA00645B

Mencer, D. E Jr., Hess, T. R., and Mebrahtu, T. (1991). Surface reactivity of titanium–aluminum alloys: Ti$_3$Al, TiAl, and TiAl$_3$. *J. Vac. Sci. Technol. A* 9, 1610–1615. doi: 10.1116/1.577669

Mo, X. H., and Jiang, W. Q. (2018). Dehydrogenation properties of LiBH$_4$ modified by Mg from first-principles calculations. *J. Alloy Compd.* 735, 668–676 doi: 10.1016/j.jallcom.2017.11.128

Mustafa, N. S., Halim-Yap, F. A., Yahya, M. S., and Ismail, M. (2018). The hydrogen storage properties and reaction mechanism of the NaAlH$_4$ + Ca(BH$_4$)$_2$ composite system. *Int. J. Hydrogen Energy* 43, 11132–11140. doi: 10.1016/j.ijhydene.2018.04.234

Naik, M., Rather, S., Zacharia, R., So, C. S., Hwang, S. W., Kim, A. R., et al. (2009). Comparative study of dehydrogenation of sodium aluminum hydride wet–doped with ScCl$_3$, TiCl$_3$, VCl$_3$, and MnCl$_2$. *J. Alloys Compd.* 471, L16–L22. doi: 10.1016/j.jallcom.2008.03.093

Orimo, S. I., Nakamori, Y., Eliseo, J. R., Züttel, A., and Jensen, C. M. (2007). Complex hydrides for hydrogen storage. *Chem. Rev.* 107, 4111–4132. doi: 10.1021/cr0501846

Schlapbach, L., and Züttel, A. (2001). Hydrogen storage materials for mobile applications. *Nature* 414, 353–358. doi: 10.1038/35104634

Vajo, J. J., Skeith, S. L., and Mertens, F. (2005). Reversible storage of hydrogen in destabilized LiBH$_4$. *J. Phys. Chem. B* 109, 3719–3722. doi: 10.1021/jp040769o

Wang, P., Kang, X. D., and Cheng, H. M. (2005). Improved hydrogen storage of TiF$_3$-doped NaAlH$_4$. *ChemPhysChem* 6, 2488–2491. doi: 10.1002/cphc.200500207

Zhang, X., Ren, Z. H., Lu, Y. H., Yao, J. H., Gao, M. X., Liu, Y. F., et al. (2018). Facile synthesis and superior catalytic activity of nano-TiN@N-C for hydrogen storage in NaAlH$_4$. *ACS Appl. Mater. Interfaces* 10, 15767–15777. doi: 10.1021/acsami.8b04011

Zhang, X., Wu, R. Y., Wang, Z. Y., Gao, M. X., Pan, H. G., and Liu, Y. F. (2016). Preparation and catalytic activity of a novel nanocrystalline ZrO$_2$@C composite for hydrogen storage in NaAlH$_4$. *Chem. Asian J.* 11, 3541–3549 doi: 10.1002/asia.201601204